

Re-purposing Compact Neuronal Circuit Policies to Govern Reinforcement Learning Tasks

Ramin M. Hasani^{1*}, Mathias Lechner^{1 2*}, Alexander Amini³, Daniela Rus,³ and Radu Grosu¹

¹Cyber Physical Systems (CPS), Technische Universität Wien (TU Wien), 1040 Vienna, Austria

²Institute of Science and Technology (IST), 3400 Klosterneuburg, Austria

³Computer Science and Artificial Intelligence Lab (CSAIL), Massachusetts Institute of Technology (MIT), Cambridge, USA

*Equal Contributions

Abstract

We propose an effective method for creating interpretable control agents, by *re-purposing* the function of a biological neural circuit model, to govern simulated and real world reinforcement learning (RL) test-beds. Inspired by the structure of the nervous system of the soil-worm, *C. elegans*, we introduce *Neuronal Circuit Policies* (NCPs) as a novel recurrent neural network instance with liquid time-constants, universal approximation capabilities and interpretable dynamics. We theoretically show that they can approximate any finite simulation time of a given continuous n -dimensional dynamical system, with n output units and some hidden units. We model instances of the policies and learn their synaptic and neuronal parameters to control standard RL tasks and demonstrate its application for autonomous parking of a real rover robot on a pre-defined trajectory. For reconfiguration of the *purpose* of the neural circuit, we adopt a search-based RL algorithm. We show that our neuronal circuit policies perform as good as deep neural network policies with the advantage of realizing interpretable dynamics at the cell-level. We theoretically find bounds for the time-varying dynamics of the circuits, and introduce a novel way to reason about networks' dynamics.

1 Introduction

Through natural evolution, the nervous system of the nematode, *C. elegans*, structured a near optimal wiring diagram (White et al. 1986). Its stereotypic brain composed of 302 neurons connected through approximately 8000 chemical and electrical synapses (Chen, Hall, and Chklovskii 2006). The functions of many neural circuits within its brain have been identified (Wicks and Rankin 1995; Chalfie et al. 1985; Li et al. 2012; Nichols et al. 2017). The general network architecture in *C. elegans* establishes a hierarchical topology from sensory neurons through upper interneuron and command interneurons down to motor neurons (See Fig. 1A). In these neuronal circuits, typically interneurons establish highly recurrent wiring diagrams with each other while sensors and command neurons mostly realize feed-forward connections to their downstream neurons. An example of such structure is a neural circuit is shown in Fig. 1B, the Tap-withdrawal (TW) circuit, which is responsible for inducing a forward/backward locomotion reflex when the worm is mechanically exposed to

touch stimulus on its body. The circuit has been characterized in terms of its neuronal dynamics (Chalfie et al. 1985). The TW circuit comprises nine neuron classes which are wired together by means of chemical and electrical synapses. Behavior of the TW reflexive response is substantially similar to the control agent's reaction in some standard control settings such as the impulse response of a controller operating on an *Inverted Pendulum* (Russell and Norvig 2010), a controller acting on driving an under-powered car, to go up on a steep hill, known as the *Mountain Car* (Singh and Sutton 1996), or a controller acting on the navigation of a rover robot that plans to go from point A to B, on a planned trajectory.

We intend to take advantage of the similarity to develop models for the circuit and assessing its performance in standard reinforcement learning (RL) and control applications. The biophysical neuronal and synaptic models form a novel recurrent neural network (RNN) structure with useful properties; 1) In addition to the nonlinearities exposed on the neurons' hidden state, the time-constant of the system varies with an additional nonlinearity originated by the synaptic model. This property results in realizing complex dynamics with fewer number of neurons compared to standard RNNs. 2) Like other RNNs, they express universal approximation capabilities, and therefore they can scale up. 3) Their dynamics are set by biophysical properties which ease the interpretation of the network hidden dynamics. 4) These network's dynamical properties such as their liquid time-constant and their hidden state are bound to a computable finite range. This feature also helps better reasoning about cells' kinetics.

In RL environments we call these networks *neuronal circuit policies* (NCP). We theoretically and experimentally investigate NCP's properties in terms of their universal approximation capability, their learning performance, their ability to solve tasks in different RL domains, and ways to interpret their internal dynamics. For this purpose, we preserve the wiring structure of an example NCP (the TW circuit) and adopt a search-based RL algorithm for neuronal and synaptic parametrization of the network.

Therefore, our principle contributions in this work can be summarized as follows:

- Demonstration of a compact neuronal circuit policy (NCP) from the brain of the *C. elegans* worm, as an interpretable liquid time-constant RNN in various RL settings. Structure of the NCPs and their semantics are presented in Sec. 2.

- Theoretic introduction of the universal approximation capability of NCPs. We introduce Theorem 1 (Sec. 3), stating that any finite-time horizon of a continuous n -dimensional dynamical system can be approximated by the hidden units and n -output units of an NCP. The theorem demonstrates the scalability of approximation capabilities of NCPs.
- Experiments with NCPs on a test-bench of different RL domains including simulated and real life applications. The RL algorithm is provided in Sec. 4, RL experiments are introduced in Sec. 5 and their results evaluated in Sec. 6.
- Interpretation of the internal dynamics of the learned policies, to quantitatively and theoretically determine bounds on the time-varying dynamics of an NCP in Lemma 1 and Lemma 2. We finally introduce a novel computational method to understand a network’s dynamics. The technique (Definition 1) determines the relation between kinetics of sensory/inter neurons and a motor neuron’s decision. We compute the magnitude of contribution, (positive or negative), of these hidden nodes to the output dynamics in determinable phases of activity, during the simulation.

2 Preliminaries

In this section, we first briefly describe the structure and dynamics of the tap-withdrawal neural circuit. We then introduce the mathematical neuron and synapse models utilized to build up the circuit, as an instance of neuronal circuit policies.

Tap-Withdrawal Neural Circuit Revisit

A mechanically exposed stimulus (i.e. tap) to the petri dish in which the worm inhabits, results in the animal’s reflexive response in the form of a forward or backward movement. This response has been named as the *tap-withdrawal reflex*, and the circuit identified to underly such behavior is known as the *tap-withdrawal* (TW) neural circuit (Rankin, Beck, and Chiba 1990). The circuit is shown in Fig. 1B. It is composed of four sensory neurons, PVD and PLM (posterior touch sensors), AVM and ALM (anterior touch sensors), four interneuron classes (AVD, PVC, AVA and AVB), and two subgroup of motor neurons which are abstracted as a forward locomotory neurons, FWD, and backward locomotory neurons, REV. Interneurons recurrently synapse into each other with excitatory and inhibitory synaptic links.

Neuron Model

Most of the neurons in *C. elegans* are observed to exhibit electrotonic dynamics (Kato et al. 2015), meaning that electric charges spread passively inside a neuron creating graded potentials. This implies that the neurons are non-spiking. Dynamics of the neurons’ membrane potential therefore, were modeled by the well-known *single-compartment membrane equation* (Koch and Segev 1998):

$$C_{m_i} \frac{dv_i}{dt} = G_{Leak_i} (V_{Leak_i} - v_i(t)) + \sum_{j=1}^n I_{in}^{(ij)}, \quad (1)$$

where C_{m_i} , G_{Leak_i} and V_{Leak_i} are parameters of the neuron and $I_{in}^{(ij)}$, stands for the external currents to the cell. We adopted Eq. (1) to govern *interneurons*’ dynamics.

For interacting with the environment, We introduced sensory and motor neuron models. A *sensory component* consists of two neurons S_p , S_n and an input variable, x . S_p gets activated when x has a positive value, whereas S_n fires when x is negative. The potential of the neurons S_p , and S_n , as a function of x , are defined by an affine function that maps the region $[x_{min}, x_{max}]$ of the system variable x , to a membrane potential range of $[-70mV, -20mV]$. (See the formula in Supplementary Materials Section 3). Note that the potential range is selected to be close to the biophysics of the nerve cells, where the resting potential, V_{Leak} , is usually set around $-60mV$ and a neuron is considered to be active when its values get higher than V_{Leak} (Hasani et al. 2017).

Similar to sensory neurons, a *motor component* is composed of two neurons M_n , M_p and a controllable motor variable y . Values of y is computed by $y := y_p + y_n$ and an affine mapping links the neuron potentials M_n and M_p , to the range $[y_{min}, y_{max}]$. (See the formula in Supplementary Materials Section 3). FWD and REV motor classes (Output units) in Fig. 1B, are modeled in this fashion.

Synapse Model

Chemical synapses are points at which two neurons trade information by the release of neurotransmitters. The chemical synaptic current depends on a non-linear component standing for their conductance strength, which is a function of the presynaptic neurons’ potential, V_j , and have a maximum weight of w_i , (standing for the maximum conductance of the synapse): (Koch and Segev 1998):

$$g(V_j) = w_i / (1 + e^{\sigma_i(V_j + \mu_i)}), \quad I_{s_{ij}} = g(V_j)(E_{ij} - V_i), \quad (2)$$

where the synaptic current linearly depends on the post-synaptic neuron’s membrane potential, V_i . By varying E , the reversal potential of the synapse, it realizes inhibitory or excitatory connection to their postsynaptic neurons.

An electrical synapse (**gap-junction**), which is a physical junction between two neurons, was modeled by a constant conductance, $\hat{\omega}_{ij}$, where based on the Ohm’s law their bidirectional current between neurons j and i , can be computed as

$$\hat{I}_{ij} = \hat{\omega}_{ij} (v_j(t) - v_i(t)). \quad (3)$$

For simulating neural networks composed of such dynamic models, we adopted an implicit numerical solver (Press et al. 2007). Formally, we realized the ODE models in a hybrid fashion which combine both implicit and explicit Euler’s method. (See Supplementary Materials Section 4, for a concrete discussion on the model implementation, and the choice of parameters.)

Note that the solver has to additionally serve as a real-time control system. For reducing the complexity therefore, our method realizes a fixed-step solver. The solver’s complexity for each time step Δ_t is $\mathcal{O}(|\# \text{ neurons}| + |\# \text{ synapses}|)$.

3 Neuronal Circuit Policies are Universal Approximators

On the theoretical strength of recurrent neural networks (RNN)s and continuous-time RNNs, it has been proved that

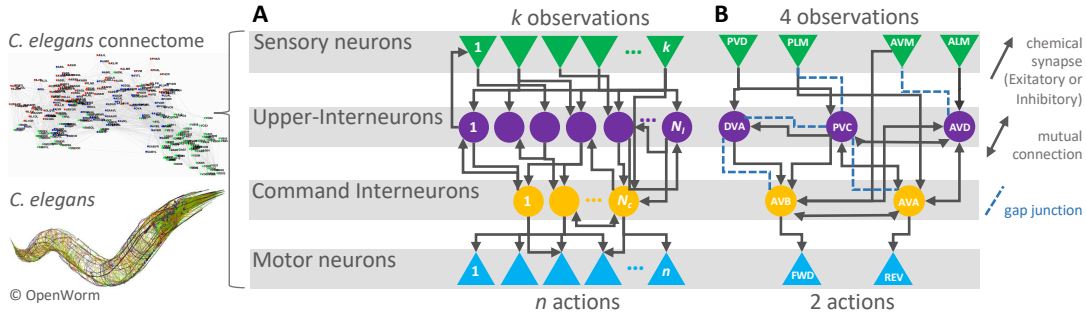


Figure 1: A) *C. elegans*' general neuronal circuit structure B) Tap-Withdrawal neural circuit schematic. Total number of interneurons = $N_i + N_C$. *C. elegans* connectome image from (Varshney et al. 2011).

any finite-time frame of a continuous mapping of a dynamical system can get approximated by the internal state of the hidden and output units of an RNN (Funahashi and Nakamura 1993). In this section, we investigate the universal approximation capability of the neuronal circuit policies.

Internal state dynamics of a neural circuit, $u(t) = [u_1(t), \dots, u_{n+N}(t)]^T$, with N interneurons (hidden units) and n motor neurons (output units) with models presented by Eq. 1 and Eq. 2, can be formulated in matrix format as:

$$\dot{u}(t) = -(1/\tau + W\sigma(u(t)))u(t) + A + W\sigma(u(t))B, \quad (4)$$

in which $\sigma(x)$ is C^1 -sigmoid functions (bounded, non-constant, continuous and monotonically increasing) and is applied element-wise. $\tau^{n+N} > 0$ is the vector including neuronal time constants, A is an $n + N$ vector of resting states, B depicts an $n + N$ vector of synaptic reversal values, and W is a $n + N$ vector produced by the matrix multiplication of a weight matrix of shape $(n + N) \times (n + N)$ and an $n + N$ vector containing the reversed value of all C_{m_i} . Both A and B entries are bound to a range $[-\alpha, \beta]$ for $0 < \alpha < +\infty$, and $0 \leq \beta < +\infty$. Note that in this formation, $\tau_i = C_{m_i}/G_{leak_i}$, A stands for a vector including all V_{leak_i}/C_{m_i} and B is a vector representing all E_{ij} s.

We prove that any given n -dimensional dynamical system for a finite simulation time, can be approximated by the internal and output states of a neuronal circuit policy, with n outputs, N interneurons and a proper initial condition. Let $x = [x_1, \dots, x_n]^T$ be the n -dimensional Euclidian space on \mathbb{R}^n .

Theorem 1. *Let S be an open subset of \mathbb{R}^n and $F : S \rightarrow \mathbb{R}^n$, be an autonomous ordinary differential equation, be a C^1 -mapping, and $\dot{x} = F(x)$ determine a dynamical system on S . Let D denote a compact subset of S and we consider the simulation of the system is bound in interval $I = [0, T]$. Then, for a positive ϵ , there exist an integer N and a neuronal circuit policy with N hidden units, n output units, such that for any rollout $\{x(t); t \in I\}$ of the system with initial value $x(0) \in D$, and a proper initial condition of the network the statement below holds:*

$$\max_{t \in I} |x(t) - u(t)| < \epsilon$$

(Comprehensive proof of Theorem 1 can be found in Supplementary Materials Section 1.).

Algorithm 1 Random Search + Objective Indicator

Input: A stochastic objective indicator f and a starting parameter θ
Output: Optimized parameter θ
 $f_\theta \leftarrow f(\theta)$
for $k \leftarrow 1$ **to** maximum iterations **do**
 $\theta' \leftarrow \theta + \text{rand}()$; $f_{\theta'} \leftarrow f(\theta')$;
 if $f_{\theta'} < f_\theta$ **then** $\theta \leftarrow \theta'$; $f_\theta \leftarrow f_{\theta'}$; $i \leftarrow 0$ **end if**;
 $i \leftarrow i + 1$
 if $i > N$ **then** $f_\theta \leftarrow f(\theta)$ **end if**;
end for
return θ

Theorem 1 suggests that neuronal circuit policies approximate arbitrary n -dimensional dynamics. To illustrate their performance experimentally, we re-purpose the TW neural circuit's dynamics to realize the continuous dynamics of standard RL tasks.

4 Search-based Reinforcement Learning

In this section we formulate an RL setting for training the parameters of a given neural circuit. The behavior of a neural circuit can be expressed as a policy $\pi_\theta(o_i, s_i) \mapsto \langle a_{i+1}, s_{i+1} \rangle$, that maps an observation o_i , and an internal state s_i of the circuit, to an action a_{i+1} , and a new internal state s_{i+1} . This policy acts upon a possible stochastic environment $Env(a_{i+1})$, that provides an observation o_{i+1} , and a reward, r_{i+1} . The stochastic return is given by $R(\theta) := \sum_{t=1}^T r_t$. The objective of the *Reinforcement learning* is to find a θ that maximizes $\mathbb{E}(R(\theta))$.

Simple search based RL (Spall 2005), as suggested in (Salimans et al. 2017), in (Duan et al. 2016), and very recently in (Mania, Guy, and Recht 2018), can scale and perform competitively with gradient based approaches, and in some cases even surpass their performance, with clear advantages such as skipping gradient scaling issues. Accordingly, we adopted a simple search-based algorithm to train the neuronal policies.

Our approach combines a *Random Search* (RS) optimization (Rastrigin 1963), with an *Objective Estimate* (OE) function $f : \theta \mapsto \mathbb{R}^+$. The OE generates N rollouts with π_θ on the environment and computes an estimate of $\mathbb{E}(R_\theta)$ based on a filtering mechanism on these N samples. We compared two filtering strategies in this context; 1) Taking the average of the N samples, and 2) taking the average of the worst k samples out of N samples.

The first strategy is equivalent to the *Sample Mean esti-*

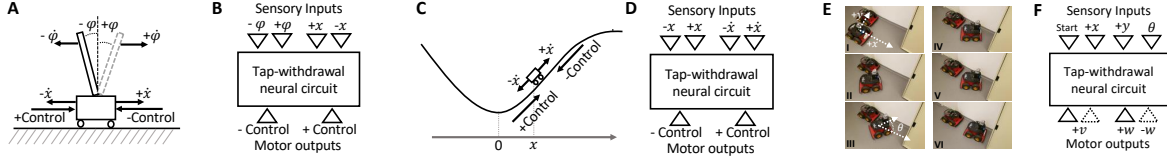


Figure 2: Mapping the environments to the TW circuit in A) Inverted pendulum, B) Mountain car, and C) Parking. See Table S3.

mator, whereas the second strategy aims to avoid getting misled by outlying high samples of $\mathbb{E}(R_\theta)$. The objective for realizing the second strategy was the fact that a suitable parameter θ makes the policy π_θ control the environment in a reasonable way even in difficult situations (i.e. rollouts with the lowest return). The algorithm is outlined in Algorithm 1.

5 Experiments

The goal of our experimentations is to answer the following questions: 1) How would a neural circuit policy perform in basic standard control settings? 2) When possible, how would the performance of our learned circuit compare to the other methods? 3) Can we transfer a policy from a simulated environment to a real environment? 4) How can we interpret the behavior of the neural circuit policies?

We prepared five environmental settings for the TW sensory/motor neurons and then deployed our RL algorithm to learn the parameters of the TW circuit and optimize the control objective. Environments include I) Inverted pendulum of Roboschool (Schulman et al. 2017), II) Mountain car of OpenAI Gym, III) Mountain car of rllab, IV) cart-pole balancing of rllab and V) Parking a real rover robot with a learned policy in a simulated environment. The code is available online.¹

The TW neural circuit (cf. Fig. 1B) allows us to incorporate 4 input observations and to take 2 output control actions. We evaluate our NCP in environments of different toolkits on a variety of dynamics, interactions and reward settings.

Inverted pendulum with the TW neural circuit

The TW neural circuit shown in Fig. 1B, contains four sensory neurons. It therefore, allows us to map the circuit to two input variables (Note that, as we discussed, a sensory component consists of two neurons for incorporating positive and negative values of the dynamic system variable). The inverted pendulum environment provides four observation variables as shown in Fig. 2A. The position of the cart x , together with its velocity \dot{x} , the angle of the pendulum φ ,² along with its angular velocity $\dot{\varphi}$.

Since the main objective of the controller is to balance the pendulum in an upward position and make the car stay within the horizontal borders, we fed φ , and x , as the inputs to the sensors of the TW circuit, as illustrated

¹Code for all experiments is available online at: https://github.com/mlech261/neuronal_circuit_policies

²Remark: The environment further splits φ into $\sin(\varphi)$ and $\cos(\varphi)$ to avoid the $2\pi \rightarrow 0$ discontinuity

in Fig. 2B. Control commands to the pendulum were originated by the abstract motor neuron classes, FWD and REV components and represented in Fig. 2B. We set up the search-based RL algorithm to optimize neurons' and synapses' parameters $\omega, \hat{\omega}, \sigma, C_m, V_{Leak}$ and G_{Leak} in the Roboschool RoboschoolInvertedPendulum-v1 environment with a slight modification (Schulman et al. 2017) in the reward calculation. It is desirable for the cart to stay in the center of the horizontal space. Therefore, we incorporated an additional axillary reward; if the pendulum is in the up-right position and in the center, an additional 20% reward is collected. This bonus linearly decreased. For instance the bonus reward is 10% if the cart is halfway to the end. Right at the borders the bonus reward vanishes. A video of different stages of the learned neuronal circuit policy for the inverted pendulum can be viewed at <https://youtu.be/iOHeQ7DhQv8>

The mountain car (OpenAI Gym) control with the TW neural circuit

In this experiment we trained the TW circuit to drive the car shown in Fig. 2C uphill to the right-hand side, by generating gravitational momentum. The observation variables are the car's horizontal position, x , together with its linear velocity. The control signal applies force to the car to build up momentum until finally reaching the top of the hill.

Similar to configuration of the inverted pendulum, we set the observational and motor variables for the tap withdrawal, as illustrated in Fig. 2D. The circuit was then learned by the search-based RL algorithm. A video illustrating the control of the car at various episodes during the learning process can be viewed at <https://youtu.be/lMrP1sXp3jk>.

The mountain car (rllab) control with the TW neural circuit

The environmental observations and motor actions for the mountain car are the same in rllab and OpenAI Gym. Therefore, we set up the TW circuit the same way we did for the mountain car in the Gym.

The major difference of the two environments are in the way the reward is computed. The environment of rllab has a graded continuous reward which is directly associated with the position of the car, whereas in the OpenAI Gym implementation, reward is sparse and gets allocated only once the car reaches a certain altitude. Furthermore, in rllab the reward is subject to a constant penalty, whereas in the Gym the penalty varies depending on the amplitude of the performed

action. Consequently, energy efficient solutions achieve a higher score in the Gym environment, while the fastest solution scores the highest in the rllab environment.

Cart-pole (rllab) control with the TW circuit

The Cart-pole environment is substantially similar to that of the inverted pendulum. In contrast to the inverted pendulum experiment, here we mapped the observation variables, pole angle, φ and the pole’s angular velocity $\dot{\varphi}$ to the sensor. As a result, the controller is not aware of the position of the cart, x , and whether the car has reached the boundaries of the movable space or not. An intuitive solution for handling more control variables would be to add sensory neurons to the TW circuit. However, in the present work we intended to maintain the structure of the TW circuit constant, and test its capabilities in control scenarios with the resulting partial observability. (See Table S3 of Supplementary for the details of mapping of the TW circuit to the environment).

Autonomous parking of the rover with the TW neural circuit

In this experiment, we generalized our TW neuronal circuit policy to a real-world control test-bed. We let the TW circuit learn to park a rover robot on a determined spot, given a set of checkpoints form a trajectory, in a deterministic simulated environment. We then deployed the learned policy on a mobile robot in a real environment shown in Fig. 2E. The key objective here was to show the capability of the method to perform well in a transformation from a simulated environment to a real setting. For doing this, we developed a *custom deterministic simulated RL environment*.¹

The rover robot provides four observational variables (start signal, position (x , y) and angular orientation θ), together with two motor actions (linear and angular velocity, v and w). We mapped all four observatory variables, as illustrated in Fig. 2F, to the sensors of the TW. Note that here the geometric reference of the surrounding space is set at the initial position of the robot. Therefore, observation variables are positive.

We mapped the linear velocity (which is a positive variable throughout the parking task) to one motor neuron and the same variable to another motor neuron. We determined two motor neurons for the positive and negative angular velocity. (See Table S3 in Supplementary for mapping details). This configuration implies that the command neuron, AVA, controls two motor neurons responsible for the turn-right and forward motion-primitives, and AVB to control the turn-left and also forward motor neurons.

RL setting for the parking task A set of checkpoints on a pre-defined parking trajectory were determined in the custom simulated environment. For every checkpoint, a deadline was assigned. At each deadline a reward was given as the negative distance of the rover to the current checkpoint. The checkpoints are placed to resemble a real parking trajectory composed of a sequence of motion primitives: Forward, turn left, forward, turn right, forward and stop. We then learned

the TW circuit, by the RL algorithm. The learned policy has been mounted on a Pioneer AT-3 mobile robot and performed a reasonable parking performance. The Video of the performance of the TW neuronal circuit policy on the parking task can be viewed at <https://youtu.be/Vwydc2ez9Wc>.

6 Experimental Evaluation

In this section, we thoroughly assess the results of our experimentation. We qualitatively and quantitatively explain the performance of our neuronal circuit policies. We then benchmark our results where possible, with the existing methods and describe the main attributes of our methodology. Finally, we quantitatively interpret dynamics of the learned policies.

Performance

The training algorithm was able to solve all five tasks, after a reasonable number of iterations as shown in Fig. 3A-E. Jumps in the learning curves of the mountain car in OpenAI Gym (Figure 3B) are the consequence of the sparse reward. The inverted pendulum of the Roboschool and the cart-pole of rllab, realized substantially similar learning curves (Figure 3A and 3D). This indicates the robustness of the policy and the learning algorithm to different frameworks for a given control task. For the deterministic parking trajectory, the learning curve converges in less than 5000 iterations.

The final return values for the basic standard RL tasks (provided in Table 1), matches that of conventional policies (Heidrich-Meisner and Igel 2008), and the state-of-the-art deep neural network policies learned by many RL algorithms (Schulman et al. 2017; Berkenkamp et al. 2017). Table 1, also depicts the average return over the entire training iterations. The average return is not significant compared to the other algorithms applied to the artificial neural network policies (Duan et al. 2016), due to fewer number of training iterations. Training curves in our case; however, reach a stable state reasonably fast in all tasks even with a fewer number of epochs.

Effect of filter size on the training performance

Fig. 4 shows how the choice of the objective-estimate, affects the training performance. The objective-estimate is defined as the mean of the k (=filter size) returns out of 20 rollouts. When $k = 20$, the estimation is equal to the *sample mean*. We tested two environments with different reward settings: The mean return of Mountaincar (OpenAI Gym) after 50,000 training iterations to represent a sparse reward scenario and the mean return of our modified inverted pendulum task after

Table 1: Training results. Return value \pm standard deviation. Performance of the learned neuronal circuit policies in terms of final return and average return over all training iterations.

| Environment | Final return | | Average return | |
|----------------------|--------------|-------------|----------------|-------------|
| Inverted pendulum | 1168.5 | \pm 21.7 | 394.1 | \pm 80.9 |
| Mountain car (Gym) | 91.5 | \pm 6.6 | 28.1 | \pm 9.6 |
| Mountain car (rllab) | -61.3 | \pm 1.4 | -196.3 | \pm 78.0 |
| Cart-pole balancing | 3716.1 | \pm 240.1 | 1230.3 | \pm 272.2 |
| Parking | -0.49 | \pm 0.63 | -6.13 | \pm 1.41 |

¹https://github.com/mlech261/neuronal_circuit_policies

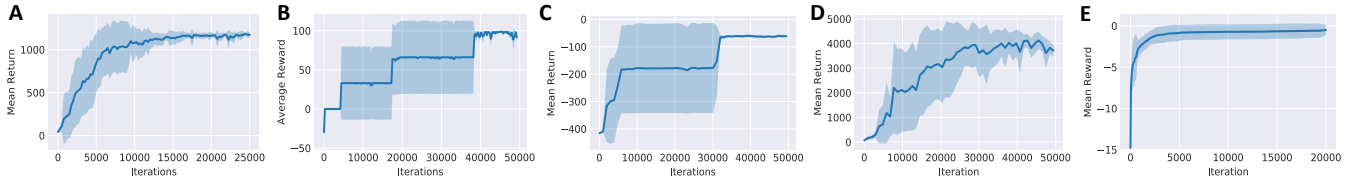


Figure 3: Learning curves for the TW circuit in standard RL tasks. A) Inverted pendulum B) Mountain car (OpenAI Gym) C) Mountain car (rllab) D) Cart-pole (rllab) E) The parking task. The shadows around the learning curves represents the standard deviation in learning each task for 10-times repetitions.

15,000 training iterations as an example of a gradual reward setting. The results denote that in a sparse reward setting, filtering of the high-outliers tend to degrade the training performance while in a gradual reward setup, filtering of the outliers improves the performance. The reported values in Fig1F, correspond to the average, when running this experiment 10 times. (Further discussions about this can be found in the Supplementary Materials Section 7).

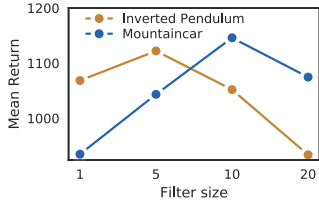


Figure 4: Filter size effect on the training performance.

Interpretability of the neuronal circuit policies

In this section, we introduce two lemmas and define a systematic approach interpreting internal dynamics of an NCP. The lemmas propose bounds on the varying time-constants of the system and the hidden state (membrane potential) of the neurons within a neural circuit. The interpretability technique determines how the kinetics of sensory neurons and interneurons relate to a motor neuron’s decision.

Lemma 1. *Let v_i denote the state of a neuron i , receiving N synaptic connections of the form Eq. 2, and P gap junctions of the form Eq. 3 from the other neurons of a network G , if dynamics of the neuron’s state be of the form Eq. 1 then the time constant of the activity of the neuron, τ_i , is bound to a range:*

$$C_i / (g_i + \sum_{j=1}^N w_{ij} + \sum_{j=1}^P \hat{w}_{ij}) \leq \tau_i \leq C_i / (g_i + \sum_{j=1}^P \hat{w}_{ij}), \quad (5)$$

(Proof in Supplementary Materials Section 9). Lemma 1 states a theoretical time-constant range in which the time-varying dynamics of each interneuron evolves in terms of its biophysical properties; thereby providing the network with the advantage of realizing complex dynamics with fewer number of elements. Fig. 5A-5C illustrates how various adaptive time constants are realized for different environmental

dynamics. Upper interneurons (particularly DVA and PVC) change their time-constants significantly compared to the other nodes. This corresponds to their contribution to various dynamical modes of the system and their ability to toggle between many dynamic phases of an output decision. As it is shown in Fig. 5A, PVC realizes a dynamic manifold with respect to the outputs of the FWD motor neuron, that depicts a periodic liquid mode-adaptation from a positive correlation phase to a negatively correlated activity. This adaptive mode-changing behavior is observed in other neurons as well (e.g., DVA in the mountain car problem, shown in Fig. 5B). Such feature for the neuronal circuit policies allows them to govern complex dynamics with smaller number of neurons and synapses. For sequential tasks such as Parking, the time-constants is not changed significantly (see Fig. 5C), since the circuit provides enough capacity to distribute dynamics amongst the system’s nodes and synapses.

Lemma 2. *Let v_i denote the state of a neuron i , receiving N synaptic connections of form Eq. 2, from the other nodes of a network G . If dynamics of the neuron’s state have the form Eq. 1, then the hidden state (membrane potential) of the neurons on a finite simulation time, $I = [0, T]$ ($0 < T < +\infty$), is bound as follows:*

$$\min(V_{leak_i}, E_{ij}^{min}) \leq v_i(t) \leq \max(V_{leak_i}, E_{ij}^{max}), \quad (6)$$

(Proof in Supplementary Materials Section 10). Lemma 2 illustrates that neuronal dynamics are bound for any input on \mathbb{R}^N . Now, given such time-varying bound dynamics, we formulate a systematic approach to determine how hidden nodes’ kinetics contribute to motor neuron decisions.

Definition 1. *Let $I = [0, T]$ be a finite simulation time of a neuronal circuit policy with k input neurons, N interneurons and n motor neurons, (Shown in Fig. 1A), acting in an RL environment. For every neuron-pair of the form (N_i, n_j) , (N_i, N_j) and (k_i, n_j) of the system, in their flattened time-series data plots (i.e. Fig. 5D) of all neuron-pairs as a function of each other, let $S = \{s_1, \dots, s_{T-1}\}$ be the set of all slopes amongst every consecutive pair points in the manifold of the neuron-pairs and $\Omega = \{\arctan(s_1), \dots, \arctan(s_{T-1})\}$ be the set of all angles in the manifold, bound in a range $[-\frac{\pi}{2}, \frac{\pi}{2}]$. Given the input dynamics, we quantify the way sensory neurons and interneurons contribute to motor neurons’ dynamics, by computing the histogram of all the manifold angles in Ω , with a bin-size equal to l (i.e. Fig 5E), as follows:*

- If the sum of the bin-counts of all $\Omega > 0$, is more than

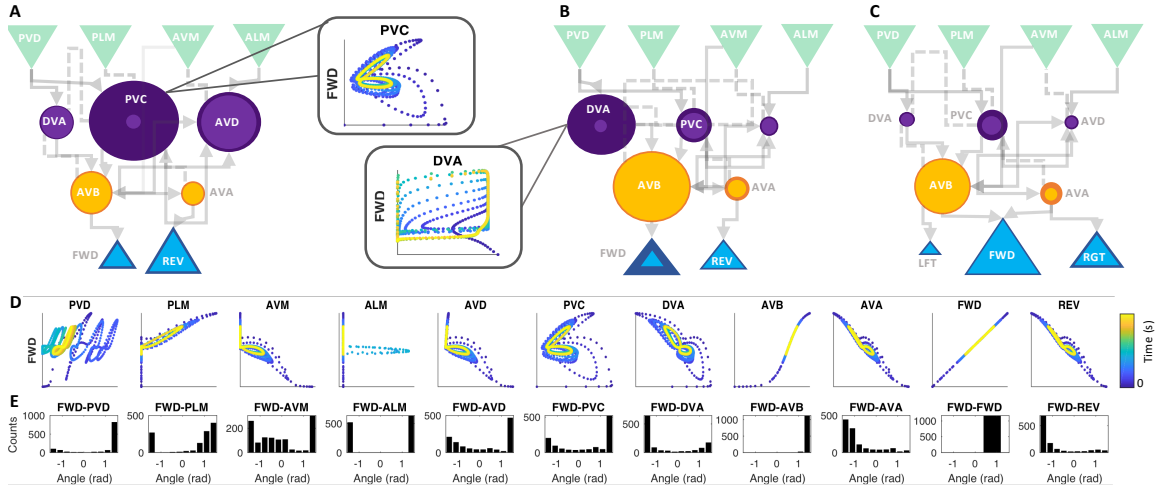


Figure 5: Interpretability analysis. Range of possible variations of the system’s time-constants for TW circuit learned for A) the inverted Pendulum, B) the mountain car, and C) the parking problem. The radius of the darker color circle, for each neuron, corresponds to the range in which the time-constant varies between τ_{min} and τ_{max} , based on Lemma 1. (See the values in Supplementary Materials, Section 12.). D) Flattened time-series data plots for one motor neuron in respect to other neurons in the Inverted pendulum problem. E) Histogram of the slopes in manifolds’ point-pair angles for a motor neuron, in the inverted pendulum task. (See Supplementary Materials Section 11, for full circuit’s analyses, in all experiments.)

half of the sum of bin-counts in the $\Omega < 0$, the overall contribution of N_i to n_j is considered to be positive.

- If the sum of bin-counts of all $\Omega < 0$, is more than half of the sum of bin-counts in the $\Omega > 0$, the overall contribution of N_i to n_j is negative,
- Otherwise, N_i contributes in phases (switching between antagonistic and phase-aligned) activity of n_j , on determinable distinct periods in I .

To exemplify the use of our interpretation method, let’s consider the neuronal activity of a learned circuit acting on an inverted pendulum for 20 seconds. In Fig. 5D, we sketched the manifolds of dynamics realized between the motor neuron FWD and all the neurons of the circuit, to quantify how the output decision is correlated to the activity of the other circuit’s neurons. Fig. 5E presents the histograms computed by using Definition 1, for the FWD motor neuron dynamics in respect to that of other neurons. Based on Definition 1, we mark sensory neurons PVD and PLM, and interneurons AVB and PVC (in certain phases) as positive contributor to the dynamics of the FWD motor neuron. We also determine AVM and AVA and obviously the REV motor neuron as the antagonistic contributors. Upper interneurons like AVD and PVC realized phase-changing dynamics where their activity toggles between a positive correlation and negative correlation, periodically. This relation is exposed by the observational inputs to the sensory neurons, as a result of the game running between the two motor neurons to keep the pole balanced on an upright position. The bounds for this activity and the phases can be seen and computed in the manifolds they make with FWD in Fig. 5D. (For the analysis of the full networks’ activities visit Supplementary Materials Section 11). Note, that command neurons AVB and AVA realized highly cor-

related activity with their downstream motor neurons. This indicates the network mostly processes the input dynamics through upper interneuron’s and forms decisive responses from command neurons to properly stimulate the motor neurons.

We observed similar attributes for the network in the mountain car and the parking problems, by using our correlation-based interpretability methodology. (See Supplementary Materials Section 11). The approach can scale to neuronal circuit policies with arbitrarily number of components. In that case, the algorithm determines important neurons in terms of neuron’s contribution to a network’s output decision in computable intervals within a finite simulation time.

7 Conclusions

We showed the performance of a novel neural information processing system, as a liquid time-constant RNN model, which we call neuronal circuit policy, in RL tasks. We theoretically showed that the circuits are universal approximators for any finite-time continuous dynamics. We selected the tap-withdrawal neural circuit of the worm as an example of the neuronal circuit policies, and governed simulated RL tasks and generalized to a real life robotic application.

We analytically and experimentally demonstrated the interpretable control performance of our learned circuits in action, and introduced a novel quantitative method to explain networks’ dynamics. The proposed method can also be utilized as a building block for the interpretability of recurrent neural networks, which despite a couple of fundamental studies (Karpathy, Johnson, and Fei-Fei 2015; Chen et al. 2016; Olah et al. 2018), is still a grand challenge to be addressed.

Finally, we open-sourced our methodologies (omitted in the review version), to encourage other researchers to further

explore the attributes of neuronal circuit policies and apply them to other control and reinforcement learning domains.

Acknowledgements

Authors would like to thank Max Tschaikowski for providing constructive feedbacks on the manuscript. This work was supported with computation resources from Microsoft Azure via the Microsoft Azure for Research program. R.M.H., M.L. and R.G. are partially supported by Horizon-2020 ECSEL Project grant No. 783163 (iDev40), and the Austrian Research Promotion Agency (FFG), Project No. 860424. A.A. is supported by the National Science Foundation (NSF) Graduate Research Fellowship Program.

References

- [Berkenkamp et al. 2017] Berkenkamp, F.; Turchetta, M.; Schoellig, A.; and Krause, A. 2017. Safe model-based reinforcement learning with stability guarantees. In *Advances in Neural Information Processing Systems 30*. Curran Associates, Inc. 908–919.
- [Chalfie et al. 1985] Chalfie, M.; Sulston, J.; White, J.; Southgate, E.; Thomson, J.; and Brenner, S. 1985. The neural circuit for touch sensitivity in *Caenorhabditis elegans*. *Journal of Neuroscience* 5(4):956–964.
- [Chen et al. 2016] Chen, X.; Duan, Y.; Houthooft, R.; Schulman, J.; Sutskever, I.; and Abbeel, P. 2016. Infogan: Interpretable representation learning by information maximizing generative adversarial nets. In *Advances in Neural Information Processing Systems*, 2172–2180.
- [Chen, Hall, and Chklovskii 2006] Chen, B. L.; Hall, D. H.; and Chklovskii, D. B. 2006. Wiring optimization can relate neuronal structure and function. *Proceedings of the National Academy of Sciences of the United States of America* 103(12):4723–4728.
- [Duan et al. 2016] Duan, Y.; Chen, X.; Houthooft, R.; Schulman, J.; and Abbeel, P. 2016. Benchmarking deep reinforcement learning for continuous control. In *International Conference on Machine Learning*, 1329–1338.
- [Funahashi and Nakamura 1993] Funahashi, K.-i., and Nakamura, Y. 1993. Approximation of dynamical systems by continuous time recurrent neural networks. *Neural networks* 6(6):801–806.
- [Hasani et al. 2017] Hasani, R. M.; Beneder, V.; Fuchs, M.; Lung, D.; and Grosu, R. 2017. Sim-ce: An advanced simulink platform for studying the brain of *caenorhabditis elegans*. *arXiv preprint arXiv:1703.06270*.
- [Heidrich-Meisner and Igel 2008] Heidrich-Meisner, V., and Igel, C. 2008. Variable metric reinforcement learning methods applied to the noisy mountain car problem. In *European Workshop on Reinforcement Learning*, 136–150. Springer.
- [Karpathy, Johnson, and Fei-Fei 2015] Karpathy, A.; Johnson, J.; and Fei-Fei, L. 2015. Visualizing and understanding recurrent networks. *arXiv preprint arXiv:1506.02078*.
- [Kato et al. 2015] Kato, S.; Kaplan, H. S.; Schrodell, T.; Skora, S.; Lindsay, T. H.; Yemini, E.; Lockery, S.; and Zimmer, M. 2015. Global brain dynamics embed the motor command sequence of *Caenorhabditis elegans*. *Cell* 163:656–669.
- [Koch and Segev 1998] Koch, C., and Segev, K. 1998. *Methods in Neuronal Modeling - From Ions to Networks*. MIT press, second edition.
- [Li et al. 2012] Li, Z.; Li, Y.; Yi, Y.; Huang, W.; Yang, S.; Niu, W.; Zhang, L.; Xu, Z.; Qu, A.; Wu, Z.; and Xu, T. 2012. Dissecting a central flip-flop circuit that integrates contradictory sensory cues in *C. elegans* feeding regulation. 3:776 EP –.
- [Mania, Guy, and Recht 2018] Mania, H.; Guy, A.; and Recht, B. 2018. Simple random search provides a competitive approach to reinforcement learning. *arXiv preprint arXiv:1803.07055*.
- [Nichols et al. 2017] Nichols, A. L.; Eichler, T.; Latham, R.; and Zimmer, M. 2017. A global brain state underlies *C. elegans* sleep behavior. *Science* 356(6344):eaam6851.
- [Olah et al. 2018] Olah, C.; Satyanarayan, A.; Johnson, I.; Carter, S.; Schubert, L.; Ye, K.; and Mordvintsev, A. 2018. The building blocks of interpretability. *Distill* 3(3):e10.
- [Press et al. 2007] Press, W. H.; Teukolsky, S. A.; Vetterling, W. T.; and Flannery, B. P. 2007. *Numerical Recipes 3rd Edition: The Art of Scientific Computing*. New York, NY, USA: Cambridge University Press, 3 edition.
- [Rankin, Beck, and Chiba 1990] Rankin, C. H.; Beck, C. D.; and Chiba, C. M. 1990. *Caenorhabditis elegans*: a new model system for the study of learning and memory. *Behavioural brain research* 37(1):89–92.
- [Rastrigin 1963] Rastrigin, L. A. 1963. About convergence of random search method in extremal control of multi-parameter systems. *Avtomat. i Telemekh.* 24:1467–1473.
- [Russell and Norvig 2010] Russell, S. J., and Norvig, P. 2010. *Artificial Intelligence: A Modern Approach*. Pearson Education, 3 edition.
- [Salimans et al. 2017] Salimans, T.; Ho, J.; Chen, X.; and Sutskever, I. 2017. Evolution strategies as a scalable alternative to reinforcement learning.
- [Schulman et al. 2017] Schulman, J.; Wolski, F.; Dhariwal, P.; Radford, A.; and Klimov, O. 2017. Proximal policy optimization algorithms. *arXiv preprint arXiv:1707.06347*.
- [Singh and Sutton 1996] Singh, S. P., and Sutton, R. S. 1996. Reinforcement learning with replacing eligibility traces. *Recent Advances in Reinforcement Learning* 123–158.
- [Spall 2005] Spall, J. C. 2005. *Introduction to stochastic search and optimization: estimation, simulation, and control*, volume 65. John Wiley & Sons.
- [Varshney et al. 2011] Varshney, L. R.; Chen, B. L.; Paniagua, E.; Hall, D. H.; and Chklovskii, D. B. 2011. Structural properties of the *caenorhabditis elegans* neuronal network. *PLoS computational biology* 7(2):e1001066.
- [White et al. 1986] White, J. G.; Southgate, E.; Thomson, J. N.; and Brenner, S. 1986. The structure of the nervous system of the nematode *Caenorhabditis elegans*. *Philosophical Transactions of the Royal Society of London B: Biological Sciences* 314(1165):1–340.

Supplementary Material

1 Proof of Theorem 1.

Internal state dynamics of a neural circuit, $u(t) = [u_1(t), \dots, u_{n+N}(t)]^T$, with N interneurons (hidden units) and n motor neurons (output units) with models presented by Eq. 1(main text) and Eq. 2(main text), can be formulated in matrix format as:

$$\dot{u}(t) = -(1/\tau + W\sigma(u(t)))u(t) + A + W\sigma(u(t))B, \quad (1)$$

in which $\sigma(x)$ is C^1 -sigmoid functions (bounded, non-constant, continuous and monotonically increasing) and is applied element-wise. $\tau^{n+N} > 0$ is the vector including neuronal time constants, A is an $n + N$ vector of resting states, B depicts an $n + N$ vector of synaptic reversal values, and W is a $n + N$ vector produced by the matrix multiplication of a weight matrix of shape $(n + N) \times (n + N)$ and an $n + N$ vector containing the reversed value of all C_{m_i} . Both A and B entries are bound to a range $[-\alpha, \beta]$ for $0 < \alpha < +\infty$, and $0 \leq \beta < +\infty$. Note that in this formation, $\tau_i = C_{m_i}/G_{leak_i}$, A stands for a vector including all V_{leak_i}/C_{m_i} and B is a vector representing all E_{ij} s.

We prove that any given n -dimensional dynamical system for a finite simulation time, can be approximated by the internal and output states of a neuronal circuit policy, with n outputs, N interneurons and a proper initial condition. Let $x = [x_1, \dots, x_n]^T$ be the n -dimensional Euclidian space on \mathbb{R}^n .

Theorem 1. *Let S be an open subset of \mathbb{R}^n and $F : S \rightarrow \mathbb{R}^n$, be an autonomous ordinary differential equation, be a C^1 -mapping, and $\dot{x} = F(x)$ determine a dynamical system on S . Let D denote a compact subset of S and we consider the simulation of the system is bound in interval $I = [0, T]$. Then, for a positive ϵ , there exist an integer N and a neuronal circuit policy with N hidden units, n output units, such that for any rollout $\{x(t); t \in I\}$ of the system with initial value $x(0) \in D$, and a proper initial condition of the network the statement below holds:*

$$\max_{t \in I} |x(t) - u(t)| < \epsilon$$

We base our poof on the fundamental universal approximation theorem (Hornik, Stinchcombe, and White 1989) on feedforward neural networks (Funahashi 1989; Cybenko 1989;

Hornik, Stinchcombe, and White 1989), recurrent neural networks (RNN) (Funahashi 1989; Schäfer and Zimmermann 2006) and time-continous RNNs (Funahashi and Nakamura 1993). We also revisit preliminary statements which are used in the proof and are about the basic facts on dynamical systems.

THEOREM (The fundamental approximation theorem) (Funahashi 1989). *Let $\sigma(x)$ be a sigmoid function (a non-constant, monotonically increasing and bounded continous function in \mathbb{R}). Let K be a compact subset of \mathbb{R}^n , and $f(x_1, \dots, x_n)$ be a continuous function on K . Then, for an arbitrary $\epsilon > 0$, there exist an integer N , real constants c_i , θ_i ($i = 1, \dots, N$) and w_{ij} ($i = 1, \dots, N; j = 1, \dots, n$), such that*

$$\max_{x \in K} |f(x_1, \dots, x_n) - \sum_{i=1}^N c_i \sigma(\sum_{j=1}^n w_{ij} x_j - \theta_i)|, \epsilon \quad (2)$$

holds.

This theorem illustrates that three-layer feedforward neural networks can approximate any continuous mapping $f : \mathbb{R}^n \rightarrow \mathbb{R}^m$ on a compact set.

THEOREM (Approximation of dynamical systems by continuous time recurrent neural networks) (Funahashi and Nakamura 1993). *Let $D \subset \mathbb{R}^n$ and $F : D \rightarrow \mathbb{R}^n$, be an autonomous ordinary differential equation, be C^1 -mapping, and $\dot{x} = F(x)$ determine a dynamical system on D . Let K denote a compact subset of D and we consider the trajectories of the system on the interval $I = [0, T]$. Then, for an arbitrary positive ϵ , there exist an integer N and a recurrent neural network with N hidden units, n output units, and an output internal state $u(t) = [U_1(t), \dots, U_n(t)]^T$, expressed as:*

$$\frac{du_i(t)}{dt} = -\frac{u_i(t)}{\tau_i} + \sum_{j=1}^m w_{ij} \sigma(u_j(t)) + I_i(t), \quad (3)$$

where τ_i is the time constant, w_{ij} are the weights, $I_i(t)$ is the input, and σ is a C^1 -sigmoid function ($\sigma(x) = 1/(1 + \exp(-x))$), such that for any trajectory $\{x(t); t \in I\}$ of the system with initial value $x(0) \in K$, and a proper initial condition of the network the statement below holds:

$$\max_{t \in I} |x(t) - u(t)| < \epsilon.$$

Note that the theorem were proved for the case where the time constants, τ , were kept constant for all hidden states and the RNN was without inputs ($I_i(t) = 0$) (Funahashi and Nakamura 1993).

We now restate the necessary concepts from the dynamical systems to be used in the proof. Where necessary, we adopt modifications and extensions to the Lemmas, for proving Theorem 1.

Lipschitz. The mapping $F : S \rightarrow \mathbb{R}^n$, where S is an open subset of \mathbb{R}^n , is called Lipschitz on S , if there exist a constant L (lipschitz constant), such that:

$$|F(x) - F(y)| \leq L|x - y|, \quad \text{for all } x, y \in S. \quad (4)$$

Locally Lipschitz. If every point of S has neighborhood S_0 in S , such that the restriction $F|_{S_0}$ is Lipschitz, then F is locally Lipschitz.

Lemma 1. Let a mapping $F : S \rightarrow \mathbb{R}^n$ be C^1 . Then F is locally Lipschitz. Also, if $D \subset S$ is compact, then the restriction $F|_D$ is Lipschitz. (Proof in (Hirsch and Smale 1973), chapter 8, section 3).

Lemma 2. Let $F : S \rightarrow \mathbb{R}^n$ be a C^1 -mapping and $x_0 \in S$. There exists a positive a and a unique solution $x : (-a, a) \rightarrow S$ of the differential equation

$$\dot{x} = F(x), \quad (5)$$

which satisfies the initial condition $x(0) = x_0$. (Proof in (Hirsch and Smale 1973), chapter 8, section 2, Theorem 1.)

Lemma 3. Let S be an open subset of \mathbb{R}^n and $F : S \rightarrow \mathbb{R}^n$ be a C^1 -mapping. On a maximal interval $J = (\alpha, \beta) \subset \mathbb{R}$, let $x(t)$ be a solution. Then for any compact subset $D \subset S$, there exists some $t \in (\alpha, \beta)$, for which $x(t) \notin D$. (Proof in (Hirsch and Smale 1973), Chapter 8, section 5, Theorem).

Lemma 4. For an $F : \mathbb{R}^n \rightarrow \mathbb{R}^n$ which is a bound C^1 -mapping, the differential equation

$$\dot{x} = -\frac{x}{\tau} + F(x), \quad (6)$$

where $\tau > 0$ has a unique solution on $[0, \infty)$. (Proof in (Funahashi and Nakamura 1993), Section 4, Lemma 4).

Lemma 5. for an $F : \mathbb{R}^n \rightarrow \mathbb{R}^n$ which is a bounded C^1 -mapping, the differential equation

$$\dot{x} = -(1/\tau + F(x))x + A + BF(x), \quad (7)$$

in which τ is a positive constant, and A and B are constants coefficients bound to a range $[-\alpha, \beta]$ for $0 < \alpha < +\infty$, and $0 \leq \beta < +\infty$, has a unique solution on $[0, \infty)$.

Proof. Based on the assumptions, we can take a positive M , such that

$$0 \leq F_i(x) \leq M (\forall i = 1, \dots, n) \quad (8)$$

by looking at the solutions of the following differential equation:

$$\dot{y} = -(1/\tau + M)y + A + BM, \quad (9)$$

we can show that

$$\min\{|x_i(0)|, \frac{\tau(A + BM)}{1 + \tau M}\} \leq x_i(t) \leq \max\{|x_i(0)|, \frac{\tau(A + BM)}{1 + \tau M}\}, \quad (10)$$

if we set the output of the max to C_{max_i} and the output of the min to C_{min_i} and also set $C_1 = \min\{C_{min_i}\}$ and $C_2 = \max\{C_{max_i}\}$, then the solution $x(t)$ satisfies

$$\sqrt{n}C_1 \leq x(t) \leq \sqrt{n}C_2. \quad (11)$$

Based on Lemma 2 and Lemma 3 a unique solution exists on the interval $[0, +\infty)$. \square

Lemma 5 demonstrates that a neuronal circuit policy defined by Eq. 7, has a unique solution on $[0, \infty)$, since the output function is bound and C^1 .

Lemma 6. Let two continuous mapping $F, \tilde{F} : S \rightarrow \mathbb{R}^n$ be Lipschitz, and L be a Lipschitz constant of F . if $\forall x \in S$,

$$|F(x) - \tilde{F}(x)| < \epsilon, \quad (12)$$

holds, if $x(t)$ and $y(t)$ are solutions to

$$\dot{x} = F(x), \quad (13)$$

$$\dot{y} = \tilde{F}(x), \quad (14)$$

on some interval J , such that $x(t_0) = y(t_0)$, then

$$|x(t) - y(t)| \leq \frac{\epsilon}{L}(\exp L|t - t_0| - 1). \quad (15)$$

(Proof in (Hirsch and Smale 1973), chapter 15, section 1, Theorem 3).

Proof of the Theorem 1: Neuronal Circuit Policies are universal approximators

Proof. Using the above theories and Lemmas, we prove that neuronal circuit policies are universal approximators. For proving Theorem 1, we adopt similar steps to that of Funahashi and Nakamura on the approximation ability of continuous time RNNs (Funahashi and Nakamura 1993).

Part 1. We choose an η which is in range $(0, \min\{\epsilon, \lambda\})$, for $\epsilon > 0$, and λ the distance between \tilde{D} and boundary ∂S of S . D_η is set:

$$D_\eta = \{x \in \mathbb{R}^n; \exists z \in \tilde{D}, |x - z| \leq \eta\}. \quad (16)$$

D_η stands for a compact subset of S , because \tilde{D} is compact. Thus, F is Lipschitz on D_η by Lemma 1. Let L_F be the Lipschitz constant of $F|_{K_\eta}$, then, we can choose an $\epsilon_l > 0$, such that

$$\epsilon_l < \frac{\eta L_F}{2(\exp L_F T - 1)}. \quad (17)$$

Based on the universal approximation theorem, there is an integer N , and an $n \times N$ matrix B , and an $N \times n$ matrix C and an N -dimensional vector μ such that

$$\max|F(x) - B\sigma(Cx + \mu)| < \frac{\epsilon_l}{2}. \quad (18)$$

We define a C^1 -mapping $\tilde{F} : \mathbb{R}^n \rightarrow \mathbb{R}^n$ as:

$$\tilde{F}(x) = -(1/\tau + W_l \sigma(Cx + \mu))x + A + W_l B \sigma(Cx + \mu), \quad (19)$$

with parameters matching that of Eq. 1 with $W_l = W$.

We set system's time constant, τ_{sys} as:

$$\tau_{sys} = \frac{1}{1/\tau + W_l \sigma(Cx + \mu)}. \quad (20)$$

We chose a large τ_{sys} , conditioned with the following:

$$(a) \quad \forall x \in D_\eta; \quad \left| \frac{x}{\tau_{sys}} \right| < \frac{\epsilon_l}{2} \quad (21)$$

$$(b) \quad \left| \frac{\mu}{\tau_{sys}} \right| < \frac{\eta L_{\tilde{G}}}{2(\exp L_{\tilde{G}} T - 1)} \text{ and } \left| \frac{1}{\tau_{sys}} \right| < \frac{L_{\tilde{G}}}{2}, \quad (22)$$

where $L_{\tilde{G}}/2$ is a lipschitz constant for the mapping $W_l \sigma : \mathbb{R}^{n+N} \rightarrow \mathbb{R}^{n+N}$ which we will determine later. To satisfy conditions (a) and (b), $\tau W_l < 1$ should hold true.

Then by Eq. 18 and 19, we can prove:

$$\max_{x \in D_\eta} |F(x) - \tilde{F}(x)| < \epsilon_l \quad (23)$$

Let's set $x(t)$ and $\tilde{x}(t)$ with initial state $x(0) = \tilde{x}(0) = x_0 \in D$, as the solutions of equations below:

$$\dot{x} = F(x), \quad (24)$$

$$\dot{\tilde{x}} = \tilde{F}(x). \quad (25)$$

Based on Lemma 6 for any $t \in I$,

$$|x(t) - \tilde{x}(t)| \leq \frac{\epsilon_l}{L_F} (\exp L_F t - 1) \quad (26)$$

$$\leq \frac{\epsilon_l}{L_F} (\exp L_F T - 1). \quad (27)$$

Thus, based on the conditions on ϵ ,

$$\max_{t \in I} |x(t) - \tilde{x}(t)| < \frac{\eta}{2}. \quad (28)$$

Part 2. Let's Considering the following dynamical system defined by \tilde{F} in Part 1:

$$\dot{\tilde{x}} = -\frac{1}{\tau_{sys}} \tilde{x} + A_1 + W_l B \sigma(C \tilde{x} + \mu). \quad (29)$$

Suppose we set $\tilde{y} = C \tilde{x} + \mu$; then:

$$\dot{\tilde{y}} = C \dot{\tilde{x}} = -\frac{1}{\tau_{sys}} \tilde{y} + E \sigma(\tilde{y}) + A_2 + \frac{\mu}{\tau_{sys}}, \quad (30)$$

where $E = C W_l B$, an $N \times N$ matrix. We define

$$\tilde{z} = [\tilde{x}_1, \dots, \tilde{x}_n, \tilde{y}_1, \dots, \tilde{y}_n]^T, \quad (31)$$

and we set a mapping $\tilde{G} : \mathbb{R}^{n+N} \rightarrow \mathbb{R}^{n+N}$ as:

$$\tilde{G}(\tilde{z}) = -\frac{1}{\tau_{sys}} \tilde{z} + W \sigma(\tilde{z}) + A + \frac{\mu_1}{\tau_{sys}}, \quad (32)$$

where;

$$W^{(n+N) \times (n+N)} = \begin{pmatrix} 0 & B \\ 0 & E \end{pmatrix}, \quad (33)$$

$$\mu_1^{n+N} = \begin{pmatrix} 0 \\ \mu \end{pmatrix}, \quad A^{n+N} = \begin{pmatrix} A_1 \\ A_2 \end{pmatrix}. \quad (34)$$

Now using Lemma 2, we can show that solutions of the following dynamical system:

$$\dot{\tilde{z}} = \tilde{G}(\tilde{z}), \quad \tilde{y}(0) = C \tilde{x}(0) + \mu, \quad (35)$$

are equivalent to the solutions of the Eq. 29.

Let's define a new dynamical system $G : \mathbb{R}^{n+N} \rightarrow \mathbb{R}^{n+N}$ as follows:

$$G(z) = -\frac{1}{\tau_{sys}} z + W \sigma(z) + A, \quad (36)$$

where $z = [x_1, \dots, x_n, y_1, \dots, y_n]^T$. Then the dynamical system below

$$\dot{z} = -\frac{1}{\tau_{sys}} z + W \sigma(z) + A, \quad (37)$$

can be realized by a neuronal circuit policy, if we set $h(t) = [h_1(t), \dots, h_N(t)]^T$ as the hidden states, and $u(t) = [U_1(t), \dots, U_n(t)]^T$ as the output states of the system. Since \tilde{G} and G are both C^1 -mapping and $\sigma'(x)$ is bound, therefore, the mapping $\tilde{z} \rightarrow W \sigma(\tilde{z}) + A$ is Lipschitz on \mathbb{R}^{n+N} , with a Lipschitz constant $L_{\tilde{G}}/2$. As $L_{\tilde{G}}/2$ is Lipschitz constant for $-\tilde{z}/\tau_{sys}$ by condition (b) on τ_{sys} , $L_{\tilde{G}}$ is a Lipschitz constant of \tilde{G} .

From Eq. 32, Eq. 36, and condition (b) of τ_{sys} , we can derive the following:

$$|\tilde{G}(z) - G(z)| = \left| \frac{\mu}{\tau_{sys}} \right| < \frac{\eta L_{\tilde{G}}}{2(\exp L_{\tilde{G}} T - 1)}. \quad (38)$$

Accordingly, we can set $\tilde{z}(t)$ and $z(t)$, solutions of the dynamical systems:

$$\dot{\tilde{z}} = \tilde{G}(z), \quad \begin{cases} \tilde{x}(0) = x_0 \in D \\ \tilde{y}(0) = C x_0 + \mu \end{cases} \quad (39)$$

$$\dot{z} = G(z), \quad \begin{cases} u(0) = x_0 \in D \\ \tilde{h}(0) = C x_0 + \mu \end{cases} \quad (40)$$

By Lemma 6, we achieve

$$\max_{t \in I} |\tilde{z}(t) - z(t)| < \frac{\eta}{2}, \quad (41)$$

and therefore we have:

$$\max_{t \in I} |\tilde{x}(t) - u(t)| < \frac{\eta}{2}, \quad (42)$$

Part3. Now by using Eq. 28 and Eq. 42, for a positive ϵ , we can design a neuronal circuit policy with internal dynamical state $z(t)$, with τ_{sys} and W . For $x(t)$ satisfying $\dot{x} = F(x)$, if we initialize the network by $u(0) = x(0)$ and $h(0) = Cx(0) + \mu$, we obtain:

$$\max_{t \in I} |x(t) - u(t)| < \frac{\eta}{2} + \frac{\eta}{2} = \eta < \epsilon. \quad (43)$$

□

REMARKS. The neuronal circuit policy allows interneurons (hidden layer) to have recurrent connections to each other, however it assumes a feed forward connection stream from hidden nodes to the motor neuron units (output units). We assumed no inputs to the system and principally showed that the interneurons' network together with motor neurons can approximate any finite trajectory of an autonomous dynamical system. The proof were performed for a neuronal circuit policy with only chemical synapses. It is easy to extend the proof for a network which includes gap junctions as well, since their contribution is a linear addition to the time constant of the system (τ_{sys}), and to the equilibrium state of a neuron, A in Eq 37.

2 Videos of the performance of the learned neuronal circuit policies

| Description | URL |
|--|---|
| TW circuit controls an inverted pendulum at different stages of the training process | https://youtu.be/i0HeQ7DhQv8 |
| TW circuit controls a mountain car at different stages of the training process | https://youtu.be/lMrPlsXp3jk |
| TW circuit performs the parking task | https://youtu.be/Vwydc2ez9Wc |
| Parking task with four degrees-of-freedom | https://youtu.be/jVQqKoHopTU |

Table S1: Videos

3 Sensory Neuron and Motor neuron equations

A **sensory component** consists of two neurons S_p , S_n and a measurable dynamic system variable, x . S_p gets activated when x has a positive value, whereas S_n fires when x is negative. Mathematically, the potential of the neurons S_p , and S_n , as a function of x , can be expressed as

$$S_p(x) := \begin{cases} -70mV & \text{if } x \leq 0 \\ -70mV + \frac{50mV}{x_{max}}x & \text{if } 0 < x \leq x_{max} \\ -20mV & \text{if } x > x_{max} \end{cases} \quad (44)$$

$$S_n(x) := \begin{cases} -70mV & \text{if } x \geq 0 \\ -70mV + \frac{50mV}{x_{min}}x & \text{if } 0 > x \geq x_{min} \\ -20mV & \text{if } x < x_{min}. \end{cases} \quad (45)$$

This maps the region $[x_{min}, x_{max}]$ of system variable x , to a membrane potential range of $[-70mV, -20mV]$. Note that the potential range is selected to be close to the biophysics of the nerve cells, where the resting potential is usually set around -70 mV and a neuron can be considered to be active when it has a potential around -20 mV (Hasani et al. 2017).

Similar to sensory neurons, a **motor component** is composed of two neurons M_n , M_p and a controllable motor

variable y . Values of y is computed by $y := y_p + y_n$ and

$$y_p(M_p) := \begin{cases} y_{max}, & \text{if } M_p > -20mV \\ \frac{y_{max}(M_p+70mV)}{50mV}, & \text{if } M_p \in [-70, -20]mV \\ 0, & \text{if } M_p < -70mV \end{cases} \quad (46)$$

$$y_n(M_n) := \begin{cases} y_{min}, & \text{if } M_n > -20mV \\ \frac{y_{min}(M_n+70mV)}{50mV}, & \text{if } M_n \in [-70, -20]mV \\ 0, & \text{if } M_n < -70mV \end{cases} \quad (47)$$

This maps the neuron potentials M_n and M_p , to the range $[y_{min}, y_{max}]$. FWD and REV motor classes of Fig. 1B (main text), are modeled in this fashion.

4 Neural Circuit Implementation and Setup

In this section we describe how to integrate the neuron and synapse equations into a computational framework to build up the TW circuit. Due to non-linearity of the sigmoid function in Eq. (7)Main-text, the neuron's differential equation, Eq. (1)Main-text, becomes non-linear. Unfortunately, there are no complete theory of solving problems of this class, explicitly (Gerald 2012). Thus, for simulating neural networks composed of such dynamic neuron models, we adopted a numerical implicit solver.

When a network structure is dense and full of synaptic pathways, the set of ODEs (neuron potentials), defined in Eq. (1)Main-text, becomes *stiff* (Press et al. 2007). Therefore, in order to overcome stability issues we used an *implicit* derivation approximation method as follows (Press et al. 2007):

$$\frac{dv}{dt} \approx \frac{v(t) - v(t - \Delta_t)}{\Delta_t} \quad \text{for some small } \Delta_t. \quad (48)$$

In this way, we discretize the time variable and transform the set of ODEs into a set of iterative equations.

For each neuron, Eq. (1)Main-text, exposed to chemical synaptic currents in the form of Eq. (7)Main-text, and gap junction currents in the form of Eq. (8)Main-text, if we apply approximation of the Eq. (48)supplementary and assume $v_{pre}(t) \approx v_{pre}(t - \Delta_t)$, we can show that the membrane potential of that neuron at time t , is computable by:

$$v(t) = \begin{aligned} & \left[\frac{C_m}{\Delta_t} v(t - \Delta_t) + G_{Leak} V_{Leak} + \right. \\ & \sum_{i \in Ex} \omega_{ex,i} E_{Rev,ex} + \sum_{i \in Inh} \omega_{inh,i} E_{Rev,inh} + \\ & \left. \sum_{i \in GJ} \omega_{gj,i} v_{pre}(t - \Delta_t) \right] / \\ & \left[\frac{C_m}{\Delta_t} + G_{Leak} + \sum_{i \in Ex} \omega_{ex,i} + \right. \\ & \left. \sum_{i \in Inh} \omega_{inh,i} + \sum_{i \in GJ} \omega_{gj,i} \right] \end{aligned} \quad (49)$$

In Eq. (49)Supplementary, $\omega_{ex,i}$, $\omega_{inh,i}$, $\omega_{gj,i}$, respectively stand for the overall conductance of the excitatory synapse, inhibitory synapse and the gap junction, where $\omega_{ex,i} = g_{ex,i}(v_{pre})$, $\omega_{inh,i} = g_{inh,i}(v_{pre})$, and $\omega_{gj,i} = \tilde{\omega}$. Variables together with their boundaries, and constants in Eq. (49)Supplementary, are summarized in the Table S2.

Table S2: Parameters and their bounds of a neural circuit

| Parameter | Value | Lower bound | Upper bound |
|----------------------|----------|-------------|-------------|
| C_m | Variable | 1mF | 1F |
| G_{Leak} | Variable | 50mS | 5S |
| E_{rev} excitatory | 0mV | | |
| E_{rev} inhibitory | -90mV | | |
| V_{Leak} | Variable | -90mV | 0mV |
| μ | -40mV | | |
| σ | Variable | 0.05 | 0.5 |
| ω | Variable | 0S | 3S |
| $\tilde{\omega}$ | Variable | 0S | 3S |

Formally, Eq. (49)Supplementary, was realized in a hybrid fashion which combine both implicit and explicit Euler's method; The overall neuron equation, Eq. (1)Main-text is approximated by the implicit Euler's method while the parts substituted from Eq. (7)Main-text and Eq. (8)Main-text, were estimated by an explicit Euler's method.

The motivation for implementing such hybrid solver, was to make the resulting algorithm of simulating the neuronal network be separable into the following steps:

1. Compute all the incoming currents, $I_{in}^{(i)}$, form all synapses to the cell using the most recent values of $v(t)$
2. Update all $v(t)$ by Eq. (49)Supplementary

This is significantly effective when implementing a neural network on a real-time controller.

5 Neuron traces for simulations included in

Figure 5

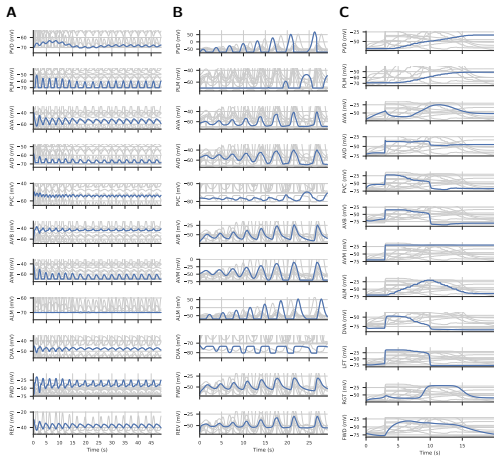


Figure S1: Neuron activity represented in figure 6. A) Inverted pendulum, B) Mountain car C) Parking

6 Experimental Setup Parameters

Mapping of the Environment to the TW Circuit (Table S3)

Experimental setup (Table S4)

With the aim of gaining a better performance, and utilizing parallel hardware resources and to increase the statistical confidence, all experiments are performed by an ensemble of 12 agents. Due to the stochasticity of the training algorithm, not all agents were able to solve the tasks in the given time frame. The observed success-rates are: Mountaincar (OpenAI gym) 25%, Mountaincar (rllab) 42%, Cart-pole 42%, Inverted Pendulum 100% and Parking 100%.

Neuron's and synapse's parameter-boundaries in the optimization setting (Table S5 and S6)

Sensory neuron mappings

As introduced in the main text, input and output values are mapped to the potential of sensory respectively motor neurons by an affine mapping. This affine mapping is defined by the minimum and maximum value of the particular input or output value. For each of the five RL environments we set these boundary values separately, according to the table S6:

7 Discussion on the influence of the filtering on the training performance

We experienced that a large filter size, i.e an objective estimate, which filters out only few outlying samples, performs better when the reward is sparse. We observed that learning curve of such environments usually has the shape of a series of step functions. One example is the Mountaincar (OpenAI Gym) environment, where a positive reward is only given once at the end, when the entire task has been solved. A large filter size performs better, in such tasks, because the episodes that have been solved by luck, are not filtered out and instead, have a large effect on the estimate. This is crucial for the training in a sparse reward setting, since during the learning phase, we observed that the agent first is unable to solve the task, then is able to solve only a few cases (e.g. when the car starts somewhere uphill) and so on, until the final agent solves the task even in the difficult scenarios.

Furthermore, we observed that a small filter size, i.e. an objective-estimate which is computed only from the lowest samples, performs slightly better in tasks with gradually increasing reward. Learning curve of such environments are usually shaped smoother. An example of such task is the pendulum (Roboschool), where a positive reward is given all the time when the pendulum is still facing upwards. Our filtering strategy performs slightly better here, because, as originally intended, the estimate is not influenced by outlying high samples. In the inverted pendulum task, such samples occur when the pendulum start in an almost straight pose and a high return can be collected without any specific action.

Table S3: Mapping the environmental variables to the sensory and motor neurons of the TW circuit, in different experiments

| Experiment | Environment variable | Type | Positive neuron | Negative neuron |
|---------------------------|----------------------|---------------------------------|-----------------|-----------------|
| Inverted Pendulum | φ | Sensor (pendulum angle) | PLM | AVM |
| | x | Sensor (cart position) | ALM | PVD |
| | a (Control) | Motor (move right/left) | FWD | REV |
| Mountain Car (OpenAI Gym) | x | Sensor (car position) | PLM | AVM |
| | \dot{x} | Sensor (car's linear velocity) | ALM | PVD |
| | a (Control) | Motor (move right/left) | FWD | REV |
| Mountain Car (rllab) | x | Sensor (car position) | PLM | AVM |
| | \dot{x} | Sensor (car's linear velocity) | ALM | PVD |
| | a (Control) | Motor (move right/left) | FWD | REV |
| Cart-Pole | φ | Sensor (pole angle) | PLM | AVM |
| | $\dot{\varphi}$ | Sensor (pole angular velocity) | ALM | PVD |
| | a (Control) | Motor (move right/left) | FWD | REV |
| Parking of a Rover | x | Sensor (estimated x position) | PVD | |
| | y | Sensor (estimated y position) | PLM | |
| | s | Sensor (start signal) | AVM | |
| | θ | Sensor (estimated angular pose) | ALM | |
| | a_1 (Control) | Motor (angular velocity) | FWD | REV |
| | a_2 (Control) | Motor (linear velocity) | FWD/REV | |

Table S4: Experiment Parameters

| | Inverted Pendulum | Mountaincar (OpenAI Gym) | Mountaincar (rllab) | Cart-pole | Parking |
|-------------|-------------------|--------------------------|---------------------|-----------|---------|
| Iterations | 25,000 | 50,000 | 50,000 | 50,000 | 20,000 |
| Horizon | 1000 | 1000 | 500 | 500 | 320 |
| Sample size | 20 | 20 | 20 | 20 | 1 |
| Filter size | 10 | 20 | 20 | 10 | 1 |

Table S5: Types of parameters that are optimized and range of valid values

| Type | Lower bound | Upper bound |
|------------|-------------|-------------|
| ω | 0 | 3 |
| σ | 0.05 | 0.5 |
| C_m | 0.001 | 1 |
| G_{Leak} | 0.05 | 5 |
| V_{Leak} | -90 | 0 |

Table S6: Input and output boundary values used to define the affine sensory and motor mappings

| Environment | Variable | Minimum | Maximum |
|--------------------------|------------------|---------|---------|
| Inverted pendulum | x | -1 | +1 |
| | φ | -0.12 | +0.12 |
| | a | -0.3 | +0.3 |
| Mountaincar (OpenAI Gym) | x | -0.02 | +0.02 |
| | \dot{x} | -0.12 | +0.12 |
| | a | -1 | +1 |
| Mountaincar (rllab) | x | -0.8 | +0.8 |
| | \dot{x} | -1.5 | +1.5 |
| | a | -1 | +1 |
| Cart-pole | φ | -0.15 | +0.15 |
| | $\dot{\varphi}$ | -1 | +1 |
| | a | -1 | +1 |
| Parking | x | | +1 |
| | y | | +1 |
| | θ | | +1 |
| | Start signal | | +1 |
| | Linear velocity | | +1 |
| | Angular velocity | -1 | +1 |

8 TW circuit can realize more degrees of freedom

In our first parking experiment, the TW circuit is able to make a turn left and move the rover forward with only one command neuron being active. This means that the circuit is able to solve the task with having binary activation states (active, not active) of the command neuron. To test the flexibility of the TW circuit and underlying neuron model, we set up a second parking experiment. In this experimental setup, we connected the command neuron AVA to two motor neurons responsible for turning right and moving backwards, and AVB to two motor neurons responsible for turning left and moving forward. In this setup, the controller is principally able to move the robot to 4 different directions: Forward, Backward, turn left and turn right. Furthermore, the TW circuit is not able to move the rover forward and turn right with only command neuron being active. If the TW circuit tends to make a right turn and move the rover forward at the same time, (which is necessary to solve this task), the circuit must be able to do this via a synchronized cooperation of the two command neurons. With this configuration, our goal was to test whether the TW circuit can express multiple output primitives with only two command neurons, by operating them in more than two potential states. We conclude that the training algorithm was able to parametrize the TW circuit, such that the agent can keep the trajectory checkpoints, correctly. A video on this scenario can be viewed at <https://youtu.be/p0GqKf0V0Ew>.

9 Proof of Lemma 1

Lemma 7. Let v_i denote the state of a neuron i , receiving N synaptic connections of the form Eq. 2(main text), and P gap junctions of the form Eq. 3(main text) from the other neurons of a network G , if dynamics of the neuron's state be of the form Eq. 1(main text) then the time constant of the activity of the neuron, τ_i , is bound to a range:

$$C_i/(g_i + \sum_{j=1}^N w_{ij} + \sum_{j=1}^P \hat{w}_{ij}) \leq \tau_i \leq C_i/(g_i + \sum_{j=1}^P \hat{w}_{ij}), \quad (50)$$

Proof. The sigmoidal nonlinearity in Eq. 2(main text), is a monotonically increasing function, bound to a range 0 and 1:

$$0 < S(Y_j, \sigma_{ij}, \mu_{ij}, E_{ij}) < 1 \quad (51)$$

By replacing the upper-bound of S , in Eq. 3(main text) and then substituting the synaptic current in Eq. 1(main text), with its function, we have:

$$C_i \frac{dv_i}{dt} = g_i \cdot (V_{leak} - v_i) + \sum_{j=1}^N w_{ij} (E_{ij} - v_i) + \sum_{j=1}^P \hat{w}_{ij} (v_j - v_i), \quad (52)$$

$$C_i \frac{dv_i}{dt} = \underbrace{(g_i V_{leak} + \sum_{j=1}^N w_{ij} E_{ij})}_{A} + \sum_{j=1}^P \hat{w}_{ij} v_j \quad (53)$$

$$- \underbrace{(g_i + \sum_{j=1}^N w_{ij} + \sum_{j=1}^P \hat{w}_{ij})}_{B} v_i, \quad (54)$$

$$C_i \frac{dv_i}{dt} = A - B v_i. \quad (55)$$

By assuming a fixed v_j , Eq. 55 is an ordinary differential equation with solution of the form:

$$v_i(t) = k_1 e^{-\frac{B}{C_i} t} + \frac{A}{B}. \quad (56)$$

From this solution, one can derive the lower bound of the system's time constant, τ_i^{min} :

$$\tau_i^{min} = \frac{C_i}{B} = \frac{C_i}{g_i + \sum_{j=1}^N w_{ij} + \sum_{j=1}^P \hat{w}_{ij}}. \quad (57)$$

By replacing the lower-bound of S , in Eq. 52, the term $\sum_{j=1}^N w_{ij} (E_{ij} - v_i)$ becomes zero, therefore:

$$C_i \frac{dv_i}{dt} = \underbrace{(g_i V_{leak} + \sum_{j=1}^P \hat{w}_{ij} v_j)}_A - \underbrace{(g_i + \sum_{j=1}^P \hat{w}_{ij})}_{B} v_i. \quad (58)$$

Thus, we can derive the upper-bound of the time constant, τ_i^{max} :

$$\tau_i^{max} = \frac{C_i}{g_i + \sum_{j=1}^P \hat{w}_{ij}}. \quad (59)$$

□

10 Proof of Lemma 2

Lemma 8. Let v_i denote the state of a neuron i , receiving N synaptic connections of form Eq. 3(main text), from the other nodes of a network G , if dynamics of the neuron's state be of the form Eq. 1(main text), then the hidden state (membrane potential) of the neurons on a finite simulation time, $I = [0, T](0 < T < +\infty)$, is bound as follows:

$$\min_{t \in I} (V_{leak_i}, E_{ij}^{min}) \leq v_i(t) \leq \max_{t \in I} (V_{leak_i}, E_{ij}^{max}), \quad (60)$$

Proof. Let us insert $M = \max\{V_{leak_i}, E_{ij}^{max}\}$ as the membrane potential $v_i(t)$ into Eq. 52:

$$C_i \frac{dv_i}{dt} = \underbrace{g_i (V_{leak} - M)}_{\leq 0} + \sum_{j=1}^N \underbrace{w_{ij} \sigma(v_j) (E_{ij} - M)}_{\leq 0}. \quad (61)$$

Right hand side of Eq. 61, is negative based on the conditions on M , positive weights and conductances, and the fact that $\sigma(v_i)$ is also positive in \mathbb{R}^N . Therefore the left hand-side must also be negative and if we conduct an approximation on the derivative term:

$$C_i \frac{dv_i}{dt} \leq 0, \quad \frac{dv_i}{dt} \approx \frac{v(t + \delta t) - v(t)}{\delta t} \leq 0, \quad (62)$$

holds, by Substituting $v(t)$ with M , we have the following:

$$\frac{v(t + \delta t) - M}{\delta t} \leq 0 \rightarrow v(t + \delta t) \leq M \quad (63)$$

and therefore:

$$v_i(t) \leq \max_{t \in I} (V_{leak_i}, E_{ij}^{max}). \quad (64)$$

Now if we substitute the membrane potential, $V(i)$ with $m = \min\{V_{leak_i}, E_{ij}^{min}\}$, following the same methodology used for the proof of the upper bound, we can derive

$$\frac{v(t + \delta t) - m}{\delta t} \leq 0 \rightarrow v(t + \delta t) \leq m, \quad (65)$$

and therefore:

$$v_i(t) \geq \min_{t \in I} (V_{leak_i}, E_{ij}^{min}). \quad (66)$$

□

11 Flattened time-series plots and correlation detection histograms for all the experiments

Based on Definition 1, in the cross correlation domain, neurons are positively depend on each other if their manifold realizes a positive slope. Similarly, a negative slop in a flattened plot, represent a negative correlation respectively.

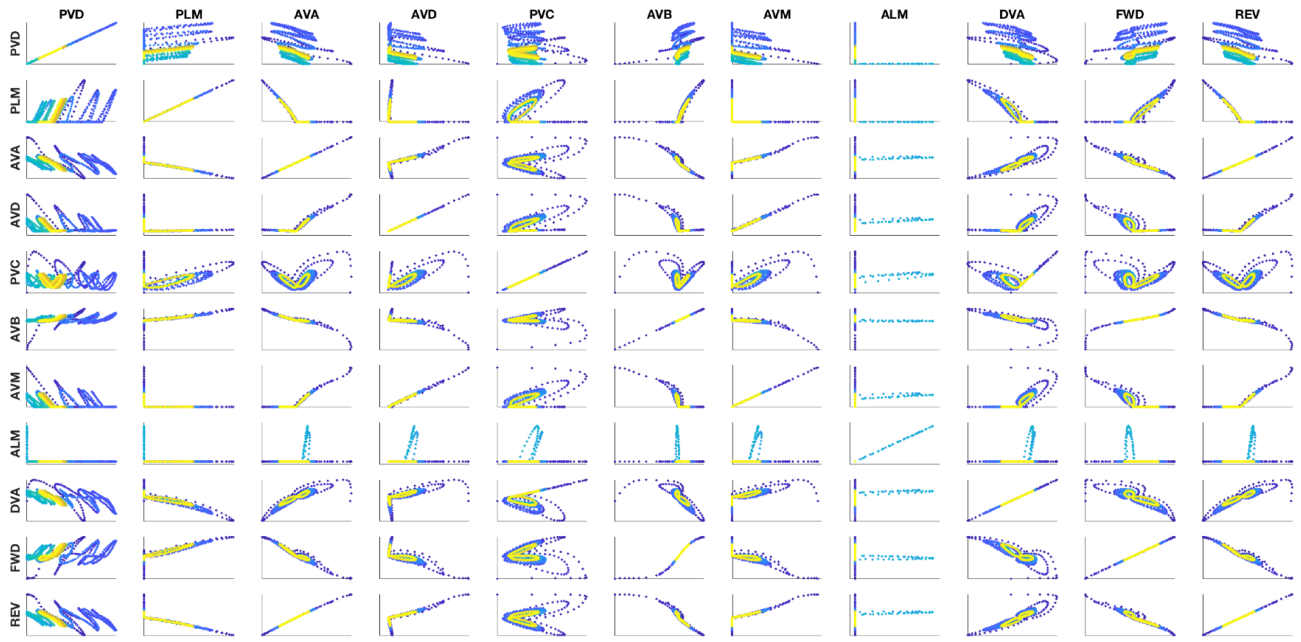


Figure S2: Flattened time-series data of neuron pairs in Inverted pendulum. The colors from dark blue to yellow, represents the evolution of simulation time in each subplot. Neuronal dynamical state is declared by the membrane potential of a neuron throughout the simulation time. Positive slopes represent positive correlation, negative slopes shows negatively correlated dynamics and a circle would realizes no correlation.

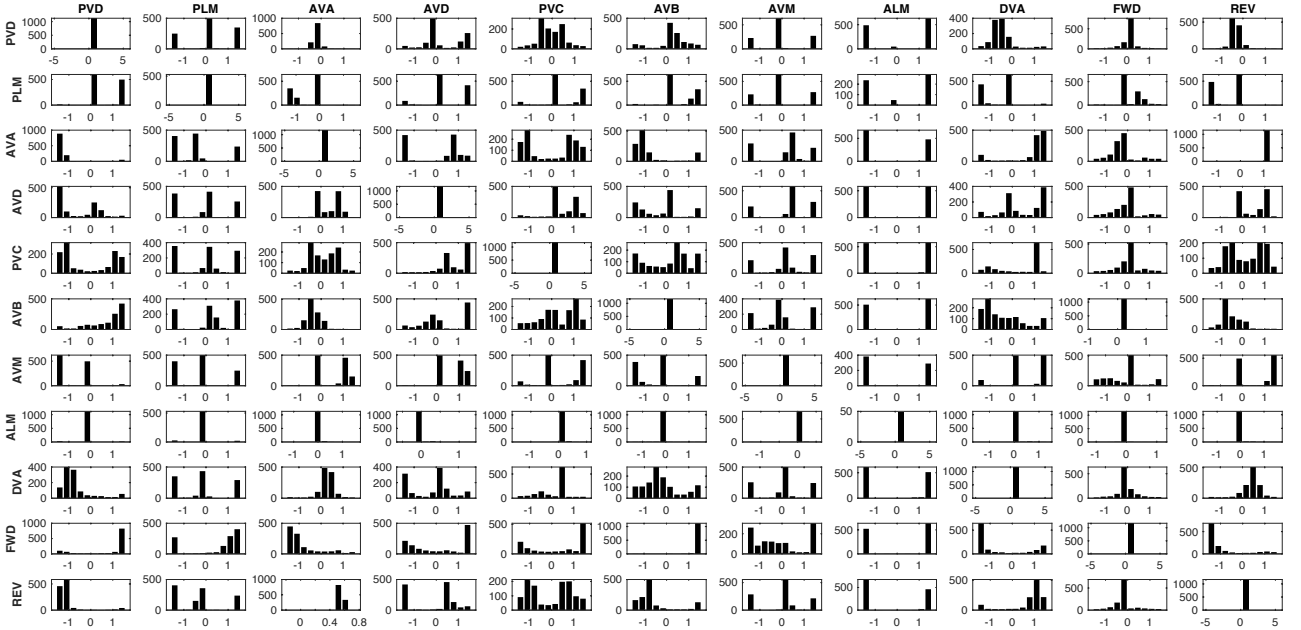


Figure S3: Neural correlation histograms in inverted pendulum. We computed the slopes between all pair data-points in the cross-correlation plots and computed their distribution for each neuron pair in order to reason about the correlation of the activity of neurons with each other. Histograms are computed with bin size of 10. Y axis stands for the slopes' counts in each bin. X axis shows the \arctan of the slope values in radian in a range $[-\pi/2, \pi/2]$. To count neurons as positive contributors to a motor neuron decision, the sum of the counts of the positive radian bins must be greater than half of the counts on the negative side.

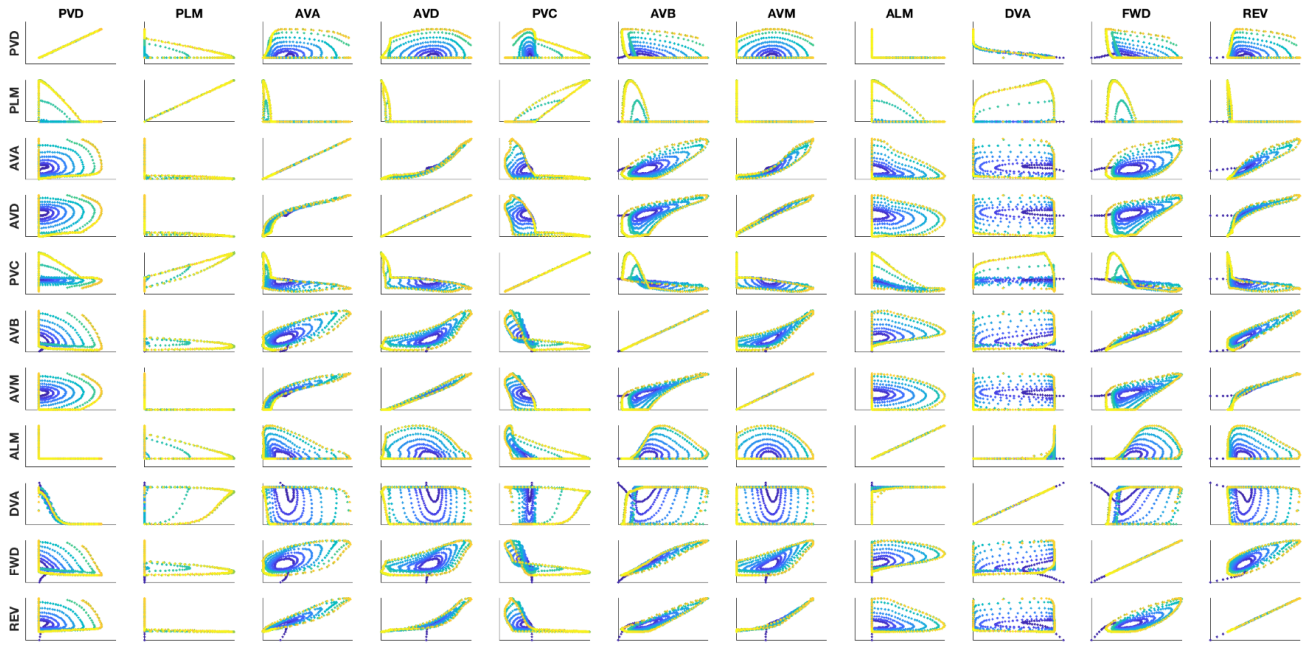


Figure S4: Flattened time-series data of neuron pairs in Mountain car. The colors from dark blue to yellow, represents the evolution of simulation time in each subplot. Neuronal dynamical state is declared by the membrane potential of a neuron throughout the simulation time. Positive slopes represent positive correlation, negative slopes shows negatively correlated dynamics and a circle would realizes no correlation.

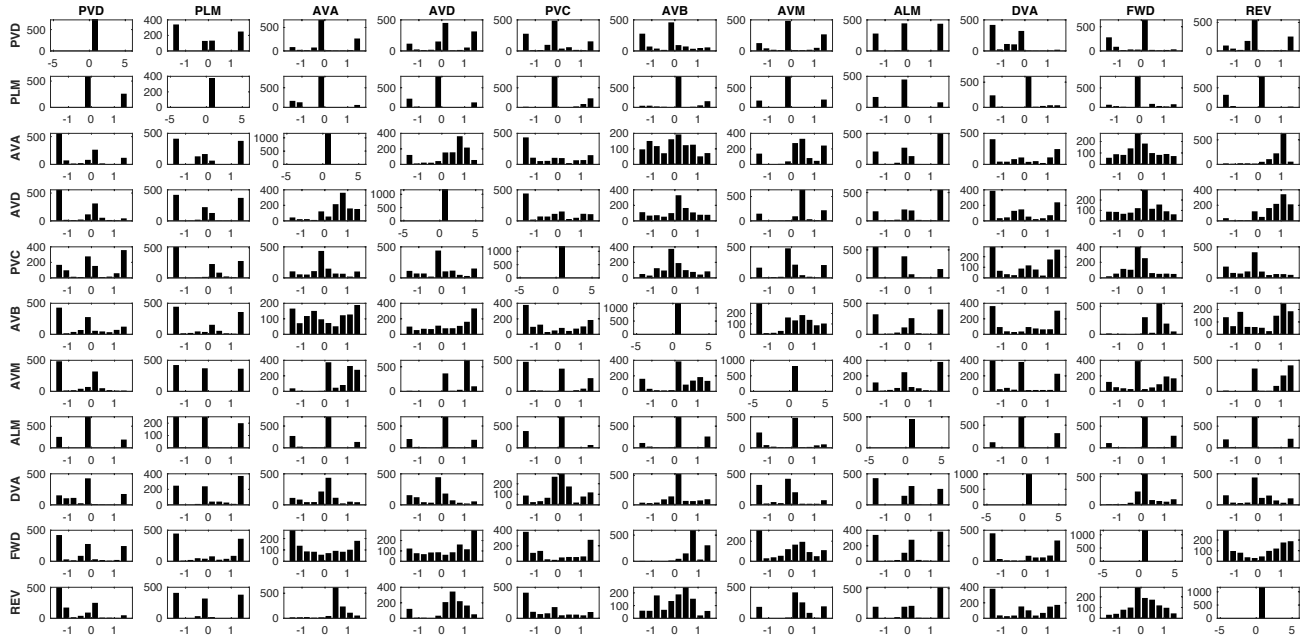


Figure S5: Neural correlation histograms in Mountain car. We computed the slopes between all pair data-points in the cross-correlation plots and computed their distribution for each neuron pair in order to reason about the correlation of the activity of neurons with each other. Histograms are computed with bin size of 10. Y axis stands for the slopes' counts in each bin. X axis shows the \arctan of the slope values in radian in a range $[-\pi/2, \pi/2]$. To count neurons as positive contributors to a motor neuron decision, the sum of the counts of the positive radian bins must be greater than half of the counts on the negative side.

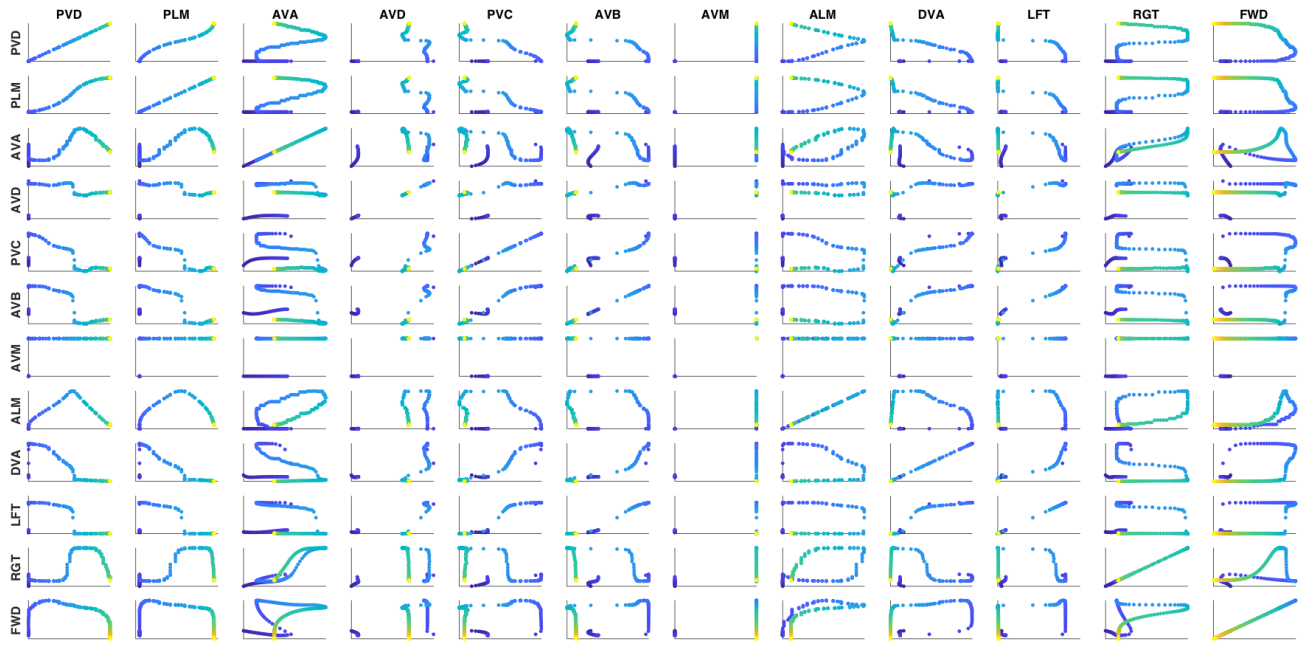


Figure S6: Flattened time-series data of neuron pairs in the parking task. The colors from dark blue to yellow, represents the evolution of simulation time in each subplot. Neuronal dynamical state is declared by the membrane potential of a neuron throughout the simulation time. Positive slopes represent positive correlation, negative slopes shows negatively correlated dynamics and a circle would realizes no correlation.

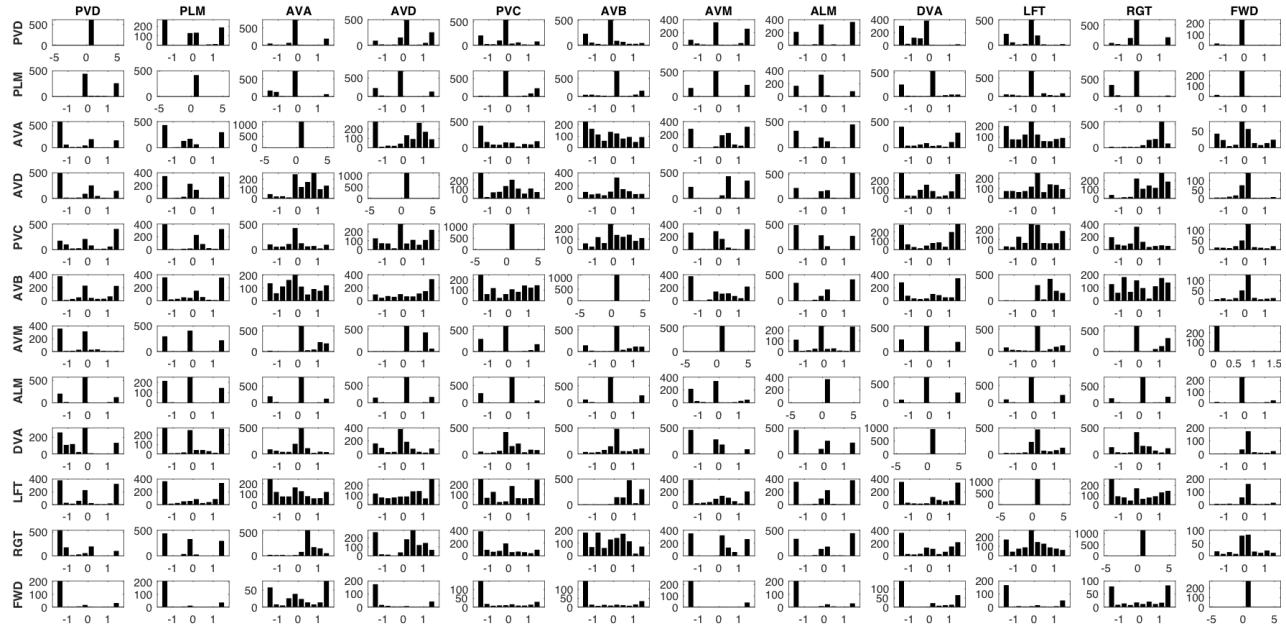


Figure S7: Neural correlation histograms in the parking task. We computed the slopes between all pair data-points in the cross-correlation plots and computed their distribution for each neuron pair in order to reason about the correlation of the activity of neurons with each other. Histograms are computed with bin size of 10. Y axis stands for the slopes' counts in each bin. X axis shows the \arctan of the slope values in radian in a range $[-\pi/2, \pi/2]$. To count neurons as positive contributors to a motor neuron decision, the sum of the counts of the positive radian bins must be greater than half of the counts on the negative side.

12 Time-constant values for the Figure 4 of [Wicks and Tsao 2015].
 Integration of mechanosensory stimuli in *Caenorhabditis elegans*. *Journal of Neuroscience* 15(3):2434–2444.

Table S7: τ_{min} and τ_{max} for the experiments based on findings of Lemma 1.

| | τ_{min} (s) | τ_{max} (s) |
|-------------------|------------------|------------------|
| Inverted Pendulum | | |
| DVA | 9.7e-4 | 2.5e-3 |
| PVC | 0.043 | 0.71 |
| AVD | 0.037 | 0.11 |
| AVB | 4.6e-3 | 4.6e-3 |
| AVA | 2.4e-4 | 3.9e-4 |
| FWD | 3.7e-4 | 2.4e-3 |
| REV | 8.7e-3 | 8.7e-3 |
| Mountain Car | | |
| DVA | 0.5 | 6.49 |
| PVC | 0.11 | 0.3 |
| AVD | 1.32e-4 | 4.75e-4 |
| AVB | 0.05 | 4.62 |
| AVA | 0.014 | 0.087 |
| FWD | 0.069 | 2.95 |
| REV | 0.47 | 0.47 |
| Parking test | | |
| DVA | 0.066 | 0.17 |
| PVC | 0.013 | 0.37 |
| AVD | 1.98e-4 | 9.65e-4 |
| AVB | 2.95 | 2.95 |
| AVA | 0.12 | 0.56 |
| LFT | 2.9e-4 | 2e-3 |
| RGT | 0.61 | 0.72 |
| FWD | 4.045 | 4.05 |

References

- [Cybenko 1989] Cybenko, G. 1989. Approximation by superpositions of a sigmoidal function. *Mathematics of control, signals and systems* 2(4):303–314.
- [Funahashi and Nakamura 1993] Funahashi, K.-i., and Nakamura, Y. 1993. Approximation of dynamical systems by continuous time recurrent neural networks. *Neural networks* 6(6):801–806.
- [Funahashi 1989] Funahashi, K.-I. 1989. On the approximate realization of continuous mappings by neural networks. *Neural networks* 2(3):183–192.
- [Gerald 2012] Gerald, T. 2012. *Ordinary Differential Equations and Dynamical Systems*, volume 140 of *Graduate Studies in Mathematics*. American Mathematical Society.
- [Hasani et al. 2017] Hasani, R. M.; Beneder, V.; Fuchs, M.; Lung, D.; and Grosu, R. 2017. Sim-ce: An advanced simulink platform for studying the brain of *caenorhabditis elegans*. *arXiv preprint arXiv:1703.06270*.
- [Hirsch and Smale 1973] Hirsch, M. W., and Smale, S. 1973. *Differential equations, dynamical systems and linear algebra*. Academic Press college division.
- [Hornik, Stinchcombe, and White 1989] Hornik, K.; Stinchcombe, M.; and White, H. 1989. Multilayer feedforward

networks are universal approximators. *Neural networks* 2(5):359–366.

[Press et al. 2007] Press, W. H.; Teukolsky, S. A.; Vetterling, W. T.; and Flannery, B. P. 2007. *Numerical Recipes 3rd Edition: The Art of Scientific Computing*. New York, NY, USA: Cambridge University Press, 3 edition.

[Schäfer and Zimmermann 2006] Schäfer, A. M., and Zimmermann, H. G. 2006. Recurrent neural networks are universal approximators. In *International Conference on Artificial Neural Networks*, 632–640. Springer.